Journal of South American Earth Sciences 101 (2020) 102654

Contents lists available at ScienceDirect

Journal of South American Earth Sciences

journal homepage: www.elsevier.com/locate/jsames

Felsic magma-water interaction in shallow intrusive environments: Timing between fluidal peperites and intrusive hyaloclastites in a jurassic cryptodome from the eastern Deseado Massif (patagonia, Argentina)

FacundoJ.De Martino[a,b,*], GerardoN. Paez[a,b], HoracioJ. Echeveste[a], SebastiánM. Jovic[a,b], Mario O.R. Tessone[a]

[a] Instituto de Recursos Minerales (INREMI), Facultad de Ciencias Naturales y Museo, UNLP, Calle 64 N 3, Esq. 120, CP 1900, La Plata, Argentina
[b] Consejo Nacional de Investigaciones Científicas y Técnicas, CONICET, Argentina

ARTICLE INFO

Keywords:
Quench fragmentation
Ductile fragmentation
Fluidization
Volcanic plumbing systems
Subvolcanic

ABSTRACT

This work describes the facies architecture, morphology and textures of a Jurassic rhyodacitic cryptodome outcropping in the Don Nicolás Mine, an important Au–Ag producing mine located in the Deseado Massif, Argentinean Patagonia. The access to 70 m deep surface mining operation and to a large number of diamond drill cores offer a unique chance to explore the volcanic rock assemblage of this body, allowing to study intrusion and growth mechanisms of a shallow subvolcanic body, and also providing insights into the timing between different brecciation processes occurring during magma intrusion into a poorly consolidated and water saturated pyroclastic sequence. Facies analysis allowed to infer this body as the result of a rhyodacitic magma intruding in a single and steady endogenous inflation pulse, resulting in the development of a flow banded core and a fluidal peperite envelope due to the combination of relatively low magma viscosities (for a rhyodacitic melt), the development of stable vapor films insulating the flowing magma and also allowing the ductile deformation of the rhyodacite clasts, and the fluidization of the unconsolidated and water saturated host rocks. After the main inflation stage stopped, the collapse of the vapor films resulted in quench fragmentation modifying the originally fluidal shape of many clast at the peperites, specially at the outer portion of the breccia envelope where fluidal clast shapes were almost completely erased due to this process. At the same time water invaded the inner portions of the intrusion, causing widespread quenching and the development of intrusive hyaloclastites at the edges of the coherent facies.

1. Introduction

Subvolcanic intrusions group a series of igneous bodies that constitute the shallow parts of volcanic plumbing systems, they can develop a wide variety of shapes and appear either isolated or forming clusters with a wide range of complexities (Cas and Wright, 1988; Sigurdsson, 2015; Schmiedel et al., 2017; Rocchi and Breitkreuz, 2017). They allow the magma to be stored and/or transported between different emplacement levels and/or to the surface (Cas and Wright, 1988; Sigurdsson, 2015). Also, they are relevant in the development of shallow hydrothermal systems as they constitute persistent heat anomalies that can drive hydrothermal circulation for long periods of time (Wohletz and Heiken, 1992; Rissmann et al., 2011). Therefore, in some instances, they may lead to the development of mineralized epithermal systems of economic relevance (Sillitoe and Bonham, 1984).

During emplacement, and depending on the magma and host rock properties, these bodies may develop extensive brecciated selvages toward their outer contacts (e.g. Cas and Wright, 1988; McPhie et al., 1993; Sigurdsson, 2015) which result from the interplay of different processes including dynamic stress (forming autobreccias; e.g., Goto et al., 2004; Yoshihiko and Akihiko, 2019), thermal stress (leading to the development of intrusive hyaloclastites; e.g. Van Otterloo et al., 2015; Páez et al., 2018) and/or fluidization (resulting in peperite formation; e.g., Németh et al., 2008; White et al., 2015; Páez et al., 2018). In these breccia envelopes, clast geometry, clast/matrix ratio and the nature of the matrix itself, along with the distribution and geometry of the different facies, have been proven to be useful tools in order to assess the intrusion mechanisms, providing also information on the

* Corresponding author. Instituto de Recursos Minerales (INREMI), Facultad de Ciencias Naturales y Museo, UNLP. Calle 64 n 3 esq. 120, CP 1900, La Plata, Argentina.
E-mail addresses: facundodemartino@yahoo.com, facundodemartino@fcnym.unlp.edu.ar (F.D. Martino).

https://doi.org/10.1016/j.jsames.2020.102654
Received 13 March 2020; Received in revised form 15 May 2020; Accepted 18 May 2020
Available online 28 May 2020
0895-9811/ Published by Elsevier Ltd.

consolidated vs. unconsolidated nature of the host rocks, the viscosity of the intruding magma among other parameters (e.g. Goto and McPhie, 1998; Stewart and McPhie, 2003; Popkhadze et al., 2014B; Páez et al., 2018; Goto and Tomiya, 2019; Cole et al., 2020).

In this work we explore the facies architecture, morphology and textures of a Jurassic rhyodacitic cryptodome outcropping in the Don Nicolás Mine, an important Au–Ag producing mine located in the Eastern Deseado Massif, a region of southern Argentina characterized by widespread presence of epithermal deposits (Schalamuk et al., 1997; Fernandez et al., 2008). Although the presence of cryptodomes in the Deseado Massif has already been mentioned (e.g. Guido, 2004), access to a 70 m deep surface mining operation along with a large number of diamond drill cores, offers a chance to explore the 3D architecture of this type of bodies, providing insights into intrusion and growth mechanisms of shallow subvolcanic bodies and allowing for a unique opportunity to explore the timing of different brecciation processes occurring during magma intrusion into poorly consolidated and water saturated sediments.

2. Methodology

Field work was focused on detailed geological mapping (1:1000, Fig. 2a) and logging of drill-cores (1:100, Fig. 2b). For the map, the Armadillo open-pit was surveyed using a Phantom 4 Pro drone in order to generate a high spatial resolution image (2 cm) for use as a base for the geological information. In order to georeference and validate the image and samples, terrestrial control points and check points were obtained with a Stonex® total station.

During mapping, three sections were logged on the pit walls and also cores from 12 diamond drill holes were logged, totalizing over 1500 m of studied diamond cores. From these, the least altered sections were sampled for further petrographic and geochemical studies (Fig. 2b). Compositional characterization of the breccias and host rocks were determined by field and petrographic approaches and the relative abundance of crystals and matrix was done visually.

Whole rock geochemical analyses were carried out by Alex Stewart International (alexstewartinternational.com). Major elements were analyzed by ICP-OES, while the trace elements were determined by ICP-MA.

3. Geological setting

The study area is located within the Martinetas district (Fig. 1), an important mining district located in the northeastern sector of the Deseado Massif, 220 km away from the city of Puerto Deseado (Figs. 1) and 40 km from the town of Tres Cerros. The area is currently mined for gold and silver by the Minera Don Nicolás S.A. mining company (MDN), producing from three discrete vein systems (Fig. 1): The Armadillo Vein System, the Choique area and the Central Vein Zone, all of which constitute a low sulfidation epithermal system composed of numerous quartz veins and stockworks (De Martino et al., 2018, 2020).

3.1. The Deseado Massif

The Deseado Massif is one of the main morfostructural regions of southern Patagonia (Fig. 1), covering a surface of about 60,000 km^2 and characterized by an extensive volcanic plateau formed during a long-lived (more than 30 Ma) magmatic event developed during Middle to Upper Jurassic times (Pankhurst and Rapela, 1995; Riley et al., 2017; Navarrete et al., 2019; Lovecchio et al., 2020) which influenced the development of numerous gold and silver deposits, leading Schalamuk et al. (1999) to define the Deseado Massif also as an Au–Ag metallogenic province.

During Jurassic times, southwestern Gondwana was affected by a voluminous magmatic event resulting in three large Igneous Provinces (LIPs), known as Karoo, Ferrar and Chon Aike (Storey et al., 1992, 2013; Storey and Kyle, 1997). With the last one covering much of the Argentinean Patagonia and Antarctic Peninsula (Kay et al., 1989; Pankhurst et al., 1998), and forming the extensive volcanic plateau that covers most of the Deseado Massif (Pankhurst and Rapela, 1995; Riley et al., 2017; Navarrete et al., 2019; Lovecchio et al., 2020). On this region, this extensive volcanism is represented by the Bahía Laura Volcanic Complex (Feruglio, 1949; Rapela and KAY, 1988; Pankhurst et al., 1993; Féraud et al., 1999; Guido, 2004). These rocks make more than 60% of the outcrops of the region and are composed mostly of pyroclastic and volcaniclastic rocks with minor domes and lava flows ranging in composition from andesites to rhyolites (Guido, 2004). Depending on its composition, the Bahía Laura Volcanic Complex has been subdivided into four formal units called Bajo Pobre, Cerro León, Chon Aike and La Matilde Formations (de Giusto et al., 1980; Panza and Haller, 2002); however, complex facies arrangement difficult the correct application of these formal units (Guido, 2004).

The widespread Jurassic volcanism and crustal extension resulted in a high thermal gradient responsible for the development of numerous hydrothermal systems (Schalamuk et al., 1997). These systems are currently represented by numerous epithermal manifestations (Fernandez et al., 2008) and associated hydrothermal paleosurfaces (sinter and travertine deposits; e.g. Guido and Campbell, 2011). Most of these mineralized systems are Au–Ag bearing low to intermediate sulfidation epithermal deposits (Guido and Schalamuk, 2003; Echavarría et al., 2005; Fernandez et al., 2008; Páez et al., 2016; Permuy Vidal et al., 2016), and are currently being exploited at eleven mines (Cerro Vanguardia, Martha, Manantial Espejo, San José, Cerro Negro, Cerro Moro, Lomada de Leiva, Martinetas, La Paloma, La Josefina and Cap-Oeste), making the Deseado Massif one of the most active mining regions of Argentina (Sillitoe, 2018; Secretaría de Política SECRETARÍA DE POLÍTICA MINERA, 2019).

3.2. The Martinetas District

The district is widely dominated by poorly exposed outcrops of the Bahía Laura Volcanic Complex, which is covered in discordance by modern alluvial and colluvial deposits (Fig. 1, De Martino et al., 2017). The area is dominated by a widespread presence of both coherent and pyroclastic volcanic units of andesitic to rhyodacitic compositions, which are later crosscut by a set of rhyolitic dykes with a NE-SW orientation (Fig. 1). The following account is based on De Martino et al. (2017) and De Martino et al. (2018).

The oldest volcanic event in the area is represented by pyroclastic rocks outcropping in the northeastern sector of Martinetas district and informally called Martinetas Ignimbrite (Fig. 1). This is a poorly sorted massive christal rich lapilli-tuff with a thickness exceeding 200 m as its base has not been intercepted by the mine drillings.

Next is an informal unit named Hydromagmatic Sequence (Figs. 1 and 3) composed of alternating centimeter to meter-thick layers of massive ignimbrites and surge deposits with tractive structures (wavy bedding, cross-stratified and planar laminations) and the presence of small fragments of coalified wood. This unit has a poor surface expression, is better developed in the Armadillo area and the Central Vein Zone (Fig. 1), and its thickness is at least one hundred and 20 m. The hydromagmatic origin of this unit was interpreted by De Martino et al. (2017) based on its thickness, the presence of accretionary lapilli, synsedimentary deformation structures and bomb impact structures (see section 4.1 for a more detailed description).

Following the previous deposits, an effusive volcanic cycle represented by rhyodacitic extrusive and subvolcanic bodies occurred in the southwestern portion of the district. This unit includes domes, cryptodomes, lava flows and several dikes, which were informally named Felsic Lavas (Fig. 1). The felsic volcanism was followed by the intrusion of a set of porphyritic subvolcanic bodies and dikes of andesitic composition (Andesitic Lavas in Fig. 1).

On top of the previous units, a poorly-sorted rhyolitic ash-flow tuff

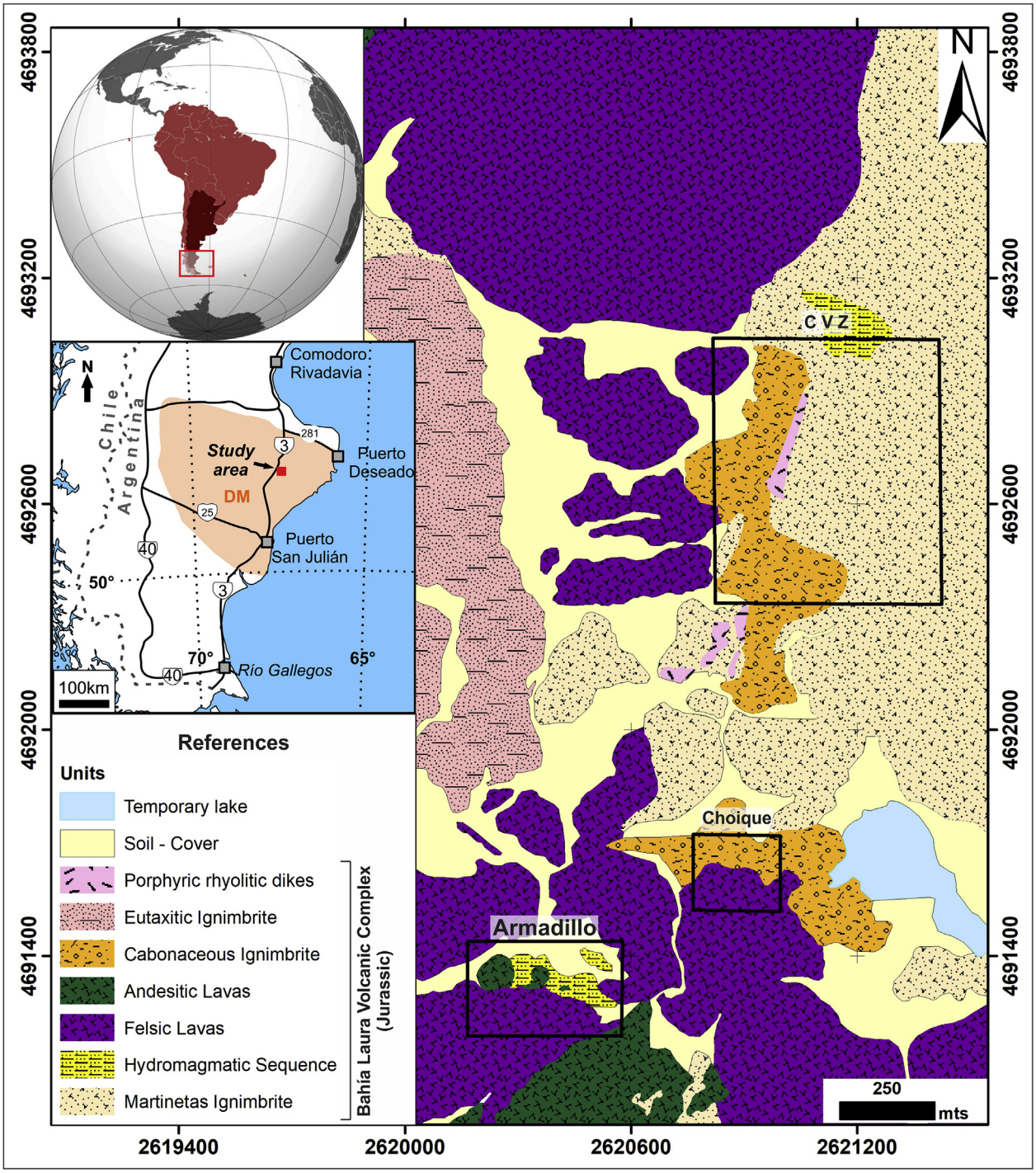

Fig. 1. Geological map of the Martinetas mining district and regional location map (insert) showing the location of the study area in the context of the Deseado Massif (light orange polygon marked as DM). The Armadillo Sector (the study area), Choique sector and Central Vein Zone sector (CVZ) are delimited by black rectangles and are the main mineralized areas within the district. Lithological references are arranged in stratigraphic order. Modified from De Martino et al. (2017). (For interpretation of the references to color in this figure legend, the reader is referred to the Web version of this article.)

informally named Carbonaceous Ignimbrite was deposited (Fig. 1). Their outcrops are closely associated with those of the Hydromagmatic Sequence and are better developed toward the north of the Choique Area and west of Central Vein Zone (Fig. 1). This unit is also characterized by the presence of coalified wood fragments.

A final pyroclastic event, the Eutaxitic Ignimbrite, overlies the previous units to the northwest of the district (Fig. 1). This is a poorly-sorted matrix supported ash-flow tuff of rhyolitic composition that is characterized by a moderate to a high degree of welding and thicknesses exceeding 50 m. Finally, an extensive swarm of porphyric rhyolitic dykes crosscut all the previous units, forming a southwest-northeast trending corridor that extends for over 10 km in length.

After the intrusion of the rhyodacites and andesites, and before the deposition of the Carbonaceous Ignimbrite, a period of intense hydrothermalism occurred in the district, giving rise to the Au–Ag epithermal deposit currently under mining (De Martino et al., 2018). The mine is operated since 2015 by Minera Don Nicolas S.A. (MDN), it has an annual production of 50,000 equivalent ounces of gold and reserves of

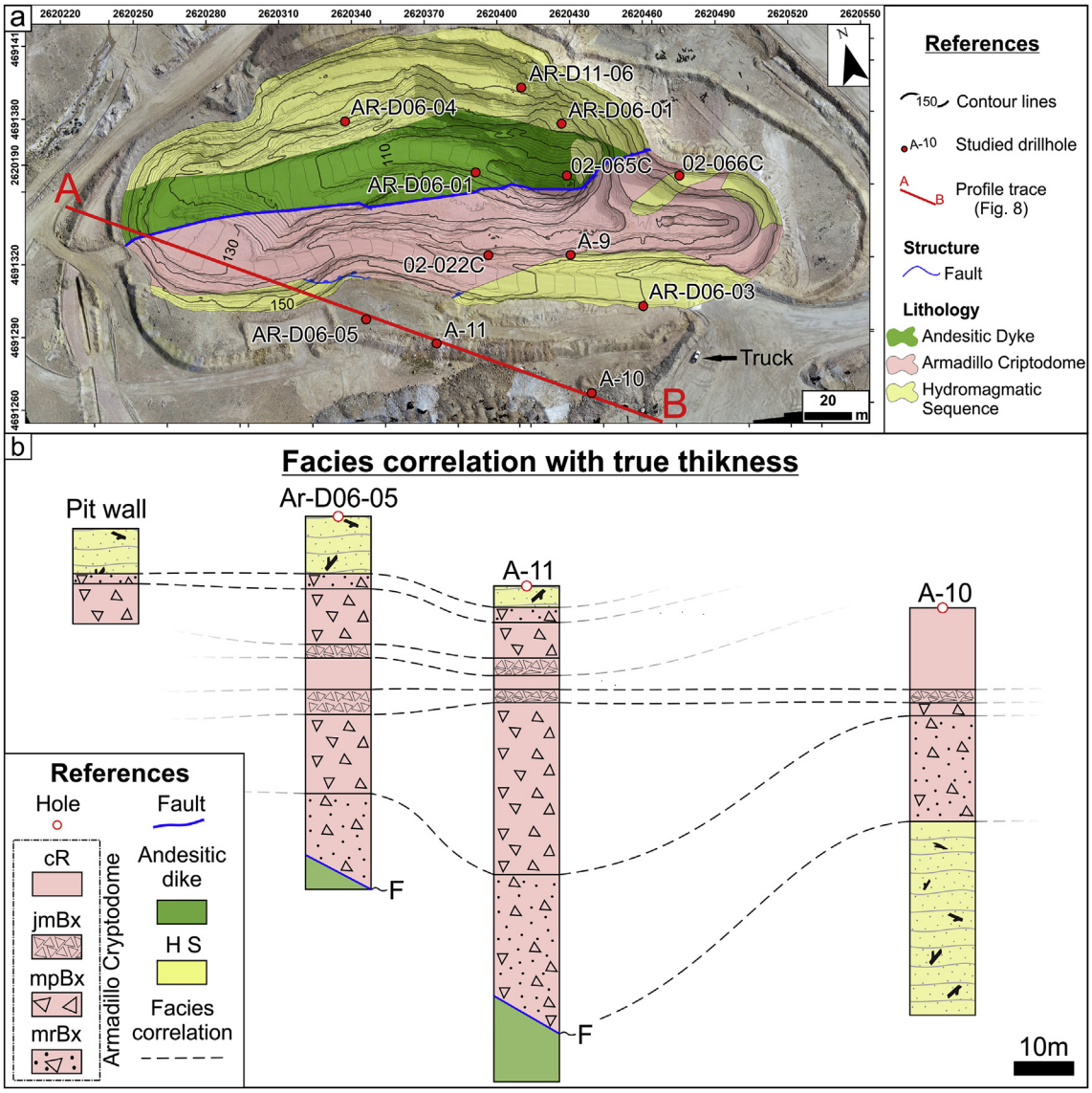

Fig. 2. a) Geological map of the Armadillo open pit showing the location of the logged drillholes and the cross section of Figs. 2b and 8b (A-B red line). b) Logs of three representative drill-cores and the pit wall showing the distribution and correlation of the facies associated with the Armadillo Cryptodome (HS: Hydromagmatic sequence). All contacts between the cryptodome facies are transitional. (For interpretation of the references to color in this figure legend, the reader is referred to the Web version of this article.)

177,100 ounces of gold and 460,800 ounces of silver distributed in four open-pits (www.mineradonnicolas.com.ar): Armadillo, Choique, Cerro Oro and Coyote, with the later ones located in the Central Vein Zone (Fig. 1). Mineralization is characterized by WNW-ESE trending quartz-adularia veins and veinlets with colloform banding and lattice bladed texture of quartz pseudomorphs after calcite (De Martino et al., 2018). Sulfide content is typically very low (< 5%) and includes only pyrite and minor chalcopyrite, with the gold mineralization being related to electrum alongside native gold and silver (De Martino et al., 2020).

4. The Armadillo cryptodome

The Armadillo open-pit is located in the south-central sector of the Martinetas District (Fig. 1) and represents one of the three main mining operations of the Don Nicolás Mine. It is an E-W elongated pit, with a length of 270 m and a maximum depth of 70 m (Fig. 2a) and it was active between 2016 and 2018. The well preserved and steep walls of this pit, and the high number of drill-holes on its surroundings offer a unique opportunity to study the three-dimensional arrangement of the volcanic rocks of the area.

At the pit walls, three units can be recognized (Fig. 2a), the oldest one corresponds to the Hydromagmatic Sequence, which hosts two different intrusive units: a rhyodacitic cryptodome, named as the Armadillo Cryptodome, and a later andesitic dike which crosscuts both units following an east-west orientation, approximately sub-parallel to the main elongation of the open-pit. On the following sections we summarize the main features of each of these units.

4.1. Hydromagmatic sequence

This unit constitutes the country rock for the studied intrusive. It is composed of an interlayering of strata of two different facies with individual thicknesses ranging between 1 and 30 cm, the total thickness of this unit exceeds a hundred of meters (up to 120 m in some drill-holes). The first of these facies (Sf-m) corresponds to massive, poorly sorted and matrix supported lapilli tuffs, consisting of up to 1 cm pumice accompanied by quartz and feldspar crystaloclasts in an ash-sized matrix. The second facies (Sf-t), is made of moderate to well-sorted fine-

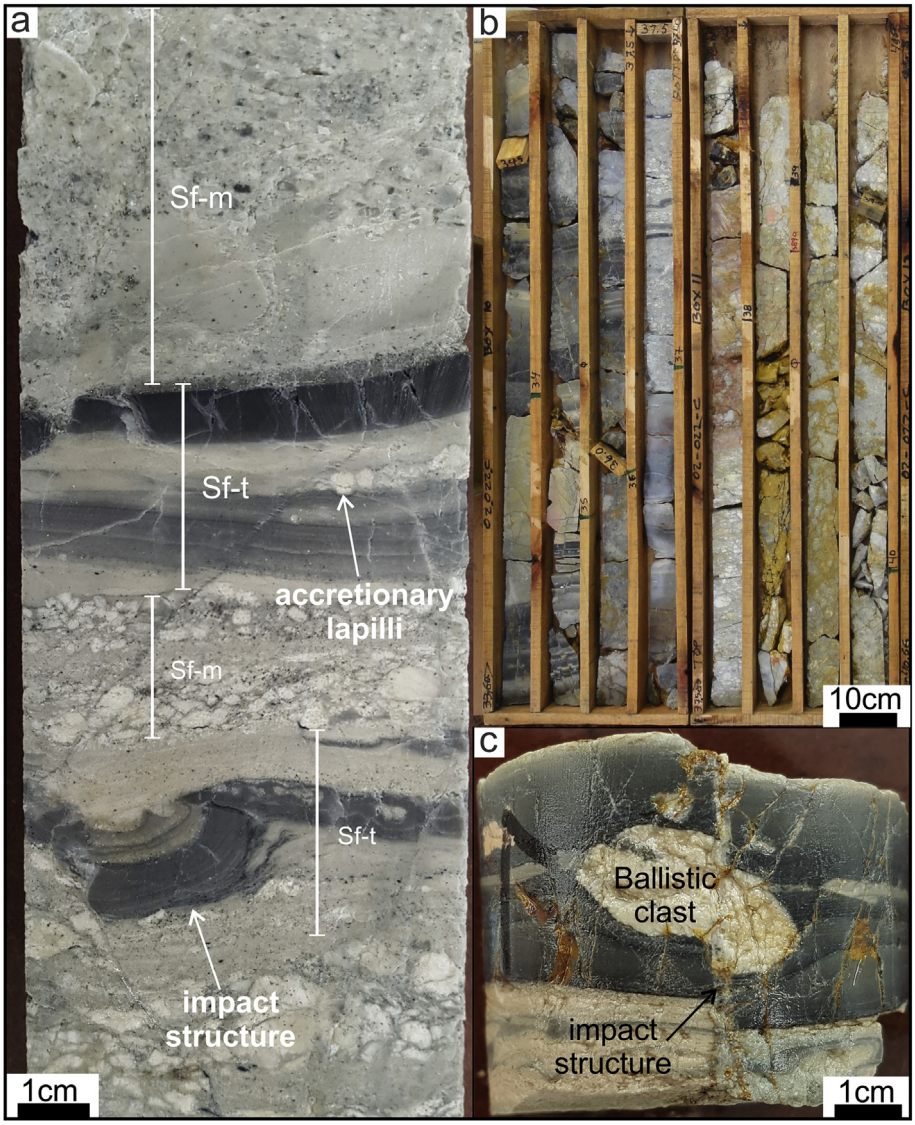

Fig. 3. Hydromagmatic Sequence. a) Drill-core of DDH 02–022C at 37 m depth showing the intercalation of facies Sf-m and Sf-t. Note the presence of an impact structure in Sf-t facies. b) Photograph of the drill cores showing the stratified structure of the Hydromagmatic Sequence. c) Drill-core photograph of DDH 02–022C at 38 m depth, where a ballistic impact sagging structure is observed in the Sf-t facies.

grained tuffs with a clast to matrix-supported texture and the presence of tractive structures such as wavy bedding, cross-stratified and planar lamination. This second facies is composed of small (1–5 mm) pumice fragments that are usually accompanied by accretionary lapilli (Fig. 3a) alongside with quartz, feldspar and mafic crystalloclasts with a moderate to an intense degree of hydrothermal alteration to white clays (feldespars) and chlorite (mafic minerals). The presence of coalified wood and ballistic impact structures is common in this facies (Fig. 3a and d).

These facies were interpreted by De Martino et al. (2017) as ignimbrites (Sf-m) and wet surges (Sf-t). According to the authors, the massive structure and poorly-sorted texture of the Sf-m facies suggest its deposition from dense pyroclastic flows. On the other hand, the high flow regime suggested by the presence of tractive structures in the Sf-t would evidence its deposition from diluted pyroclastic flows; with the presence of the accretionary lapilli and soft deformation structures (related to impact structures) evidencing high humidity values in the eruptive column, allowing the authors to interpret the Sf-t facies as the result of wet base surges (in the sense of Sheridan and Wohletz, 1983). In addition, the thick intercalation of these two facies can be related to phreatoplinian multi-episodic events, in which each phase of the eruption sequence generated its own characteristic deposits. In this scheme, the lapilli-rich layers represent some of the finest and therefore most fragmented ash beds from the wet eruption clouds and the pyroclastic flows, evidencing the collapse of the phreatoplinian eruptive column (e.g., Self, 1983; Wilson, 2001; De Rita et al., 2002; Avery et al., 2017).

In this way, we further interpret this unit as a phreatomagmatic breccia *sensu stricto* (Németh and Kósik, 2020), which originated from successive explosive eruptions caused by molten fuel-coolant interaction as the main process behind magma fragmentation occurring as a consequence of direct magma-water interaction.

4.2. Rhyodacitic intrusion (Armadillo Cryptodome)

This unit is hosted completely within the Hydromagmatic Sequence and corresponds to a subvolcanic body of rhyodacitic composition (Fig. 4d) with a microporphiritic texture and aphanitic groundmass. One of its main features is the presence of a thick breccia envelope towards its contacts with the country rocks. As this intrusion is the main focus of this work, its facies will be further discussed in the following sections.

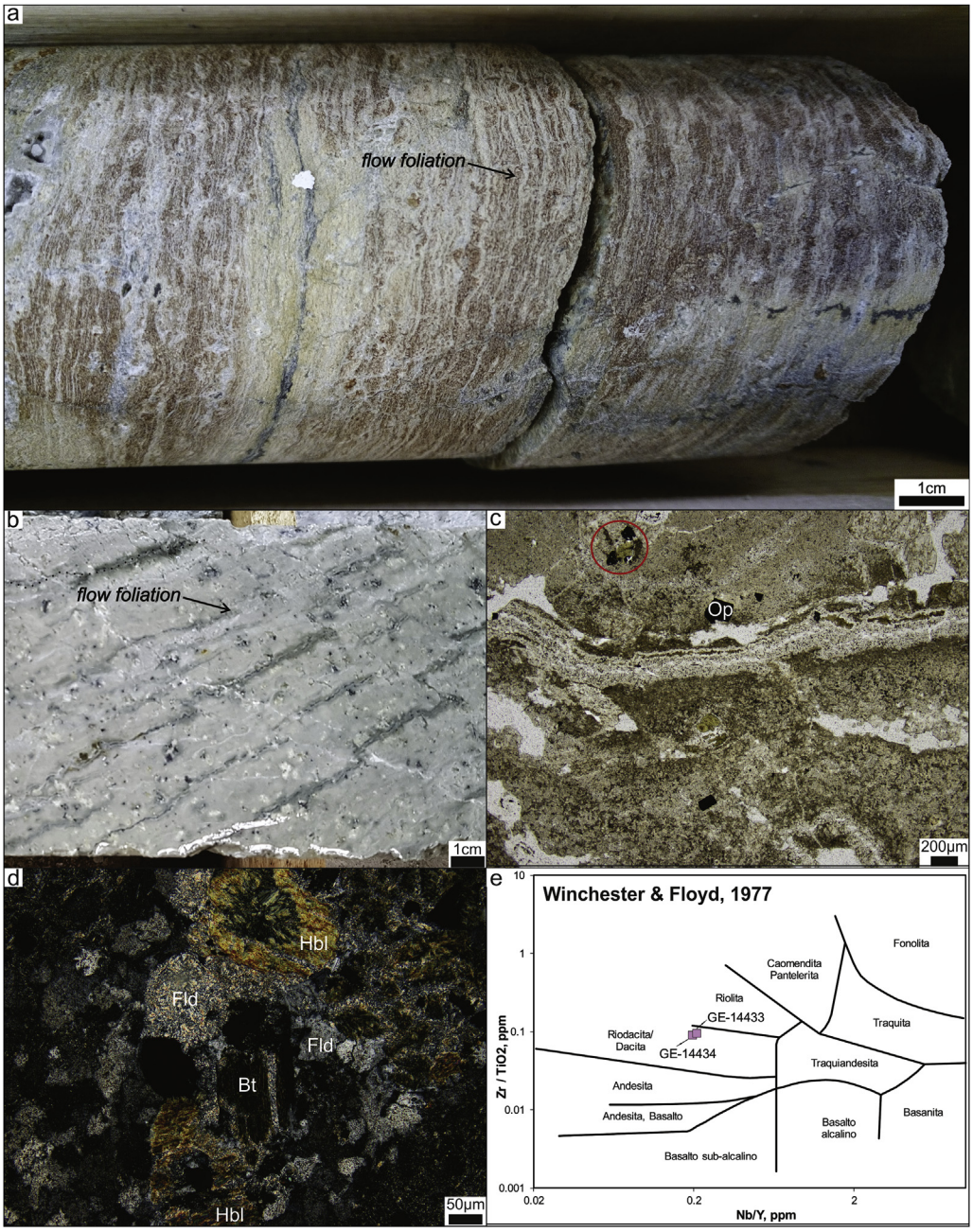

Fig. 4. Coherent rhyodacite facies (cR). a) Drill-core specimen photograph showing the flow foliation and microporphyritic texture typical of this facies. b) Detail view of a drill-core showing the flow banding and microporphic texture. c) Photomicrograph under plain-polarized light where the flow foliation and porphyritic texture are shown. Chloritized amphibole (red circle) and opaque minerals (Op) can also be identified. d) Photomicrograph under cross-polarized light of a glomeroporphyritic aggregate of alkali feldspars altered to sericite (Fld), chloritized amphiboles (Hbl) and biotites (Bt). e) Discrimination diagram Nb/Y vs. Zr/TiO_2x10,000 (according to Winchester and Floyd, 1977) showing the whole rock composition for this facies (pink squares). (For interpretation of the references to color in this figure legend, the reader is referred to the Web version of this article.)

4.3. Andesitic dike

This is the youngest unit in the pit area, is composed of andesites with a porphyritic texture with plagioclase and amphibole phenocrysts immersed in a green aphanitic groundmass. The dyke crosscut the previous units following an E-W direction and is in tectonic contact with the Armadillo Cryptodome toward its southern contact; however, its intrusive contact was confirmed while studying the drill cores. The body is characterized by sharp contacts and a massive and coherent interior, although sometimes it can incorporate up to several meter wide blocks of the Hydromagmatic Sequence.

5. Facies model of Armadillo cryptodome

By mapping the Armadillo Open Pit at 1:1000 scale (Fig. 1) and the subsequent logging of a selection of 18 drill holes of the area, it was possible to reconstruct the facies architecture of the Armadillo Cryptodome. This body is an intrusion with a relatively flat roof, a maximum thickness of about 150 m and a diameter of at least 200 m (Fig. 2). This body is part of a much more extensive dome complex, the Felsic Lavas unit defined by De Martino et al. (2017), which is developed in the immediate vicinity of the operation area of the mine (Fig. 1).

As was previously stated, the contacts between the intrusive and the country rocks are characterized by the development of a series of breccia facies. The following account summarizes the main characteristics of the four facies defined for this intrusion based on its textural and compositional characteristics.

5.1. Coherent rhyodacite facies (cR)

This facies corresponds to the unbrecciated parts of the cryptodome and is composed of a microporphyric lava with phenocrystals not exceeding 10–15% in volume (Fig. 4a, b and c), including K-feldspars

Table 1
Table of geochemical data for two samples of the Armadillo Cryptodome. *BDL: Below detection limit of the analysis.

Sample	Major elements (% weight)	SiO2	Al2O3	Fe2O3 (Total)	MgO	CaO	Na2O	K2O	TiO2	P2O5	MnO	Cr2O3	LOI	Total
GE-14433		85,1	7,38	1,47	0,09	0,05	0,12	2,66	0,12	BDL	BDL	0,002	2	98,992
GE-14434		83,45	8,26	1,86	0,07	0,06	0,18	3,23	0,16	0,01	BDL	0,002	2,2	99,482
	Trace elements (ppm)	Rb	Sr	Y	Zr	Nb	Ba	La	Ce	Pr	Nd	Sm	Eu	Tb
GE-14433		100,3	53,7	15,3	114,4	3,2	350	20,2	44,7	5,87	23,6	4,78	0,83	0,52
GE-14434		115,4	37	23,4	144,3	4,6	398	28,3	64,6	8,38	35,6	8,01	1,5	0,88
		Gd	Dy	Ho	Er	Tm	Yb	Lu	Mo	Hf	Pb	Sb	Sn	Ta
GE-14433		3,89	3,25	0,58	1,65	0,27	1,8	0,28	7,2	2,9	5,8	17,8	1	0,2
GE-14434		6,59	5,13	0,85	2,25	0,35	2,43	0,35	7,9	4	7,5	20,2	BDL	0,4

(5%) altered to sericite, biotite (1%), amphibole (3.5%) and opaque minerals (0.5%), which are immersed in a devitrified groundmass made of a fine-grained mosaic of quartz and few feldspar microlites (Fig. 4 c and d). This facies has a penetrative foliation that is accompanied by textural banding (Fig. 4a and b), where microporphyritic and aphyric bands alternate within the groundmass. In the microporphyritic domains, phenocrysts are clustered together forming glomeroporphyritic aggregates (Fig. 4 c and d). Considering the phenocryst assemblage, these rocks can be classified as andesites; however, whole rock analysis allows its classification as rhyodacites (Table 1 and Fig. 4e).

Interpretation: This facies represents the coherent (non-brecciated) interior of the cryptodome. The presence of a vitreous (now devitrified) groundmass evidence relatively high cooling rates, while the presence of flow banding is interpreted as the result of magma flowing during the emplacement of the body (McPhie et al., 1993; Llambías, 2008; Sigurdsson, 2015).

5.2. Jigsaw-fit monomictic breccias (jmBx)

This facies is composed of jigsaw-fit clasts showing little to no evidence of rotation with a moderate to poor selection and a clast to matrix-supported texture (Fig. 5a). Both clasts and matrix are made exclusively of cR derived material with blocky angular to subangular shapes with straight and curviplanar limits (Fig. 5a and b). When present, the matrix, that is partially devitrified and hydrothermally altered (Fig. 5c), generally does not exceed 10–20% in volume and is characterized black to dark green colors (Fig. 5c and d). Clast size is very variable, ranging from millimeters up to a few tens of centimeters, and shows a broad tendency to diminish in size toward the outer portions of these breccias.

This facies forms an irregular envelope completely surrounding the cR facies with a thickness that varies from a few tens of centimeters to almost 5 m (Figs. 2 and 8). Contact between these two facies is transitional, occurring by an increase in clast size toward the interior of the cryptodome, which is also accompanied by a decrease in matrix content.

Interpretation: Based on the monolithological nature of both clasts and matrix, the overall low proportion of matrix, the jigsaw-fit arrangement of clasts and its gradational contact with the mpBx facies, this facies is interpreted as intrusive hyaloclastites (McPhie et al., 1993; Van Otterloo et al., 2015; White et al., 2015), formed in the inner portions of the breccia envelope as the result of quench fragmentation as the consequence of the thermal shock occurring during the intrusion of the body.

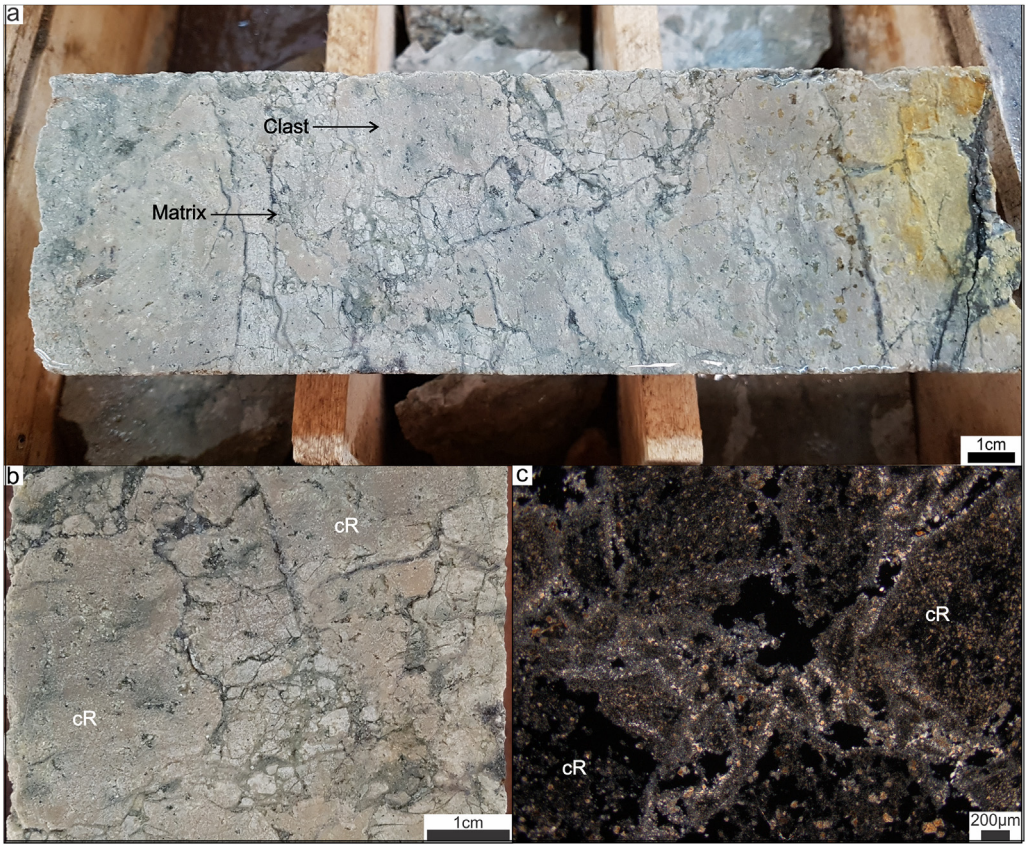

Fig. 5. Jigsaw-fit monomictic breccias (jmBx). a) Drill-core specimen showing the overall aspect of this facies. b) Detail of the breccia showing the jigsaw fit arrangement of clasts, the low proportion of matrix and the rhyodacitic lava derived clasts (cR). c) Photomicrograph under polarized light of this breccia showing jig-saw fitting clasts of rhyodacitic lava surrounded by low proportions of matrix. Both clasts and matrix show evidence of hydrothermal alteration (silicification).

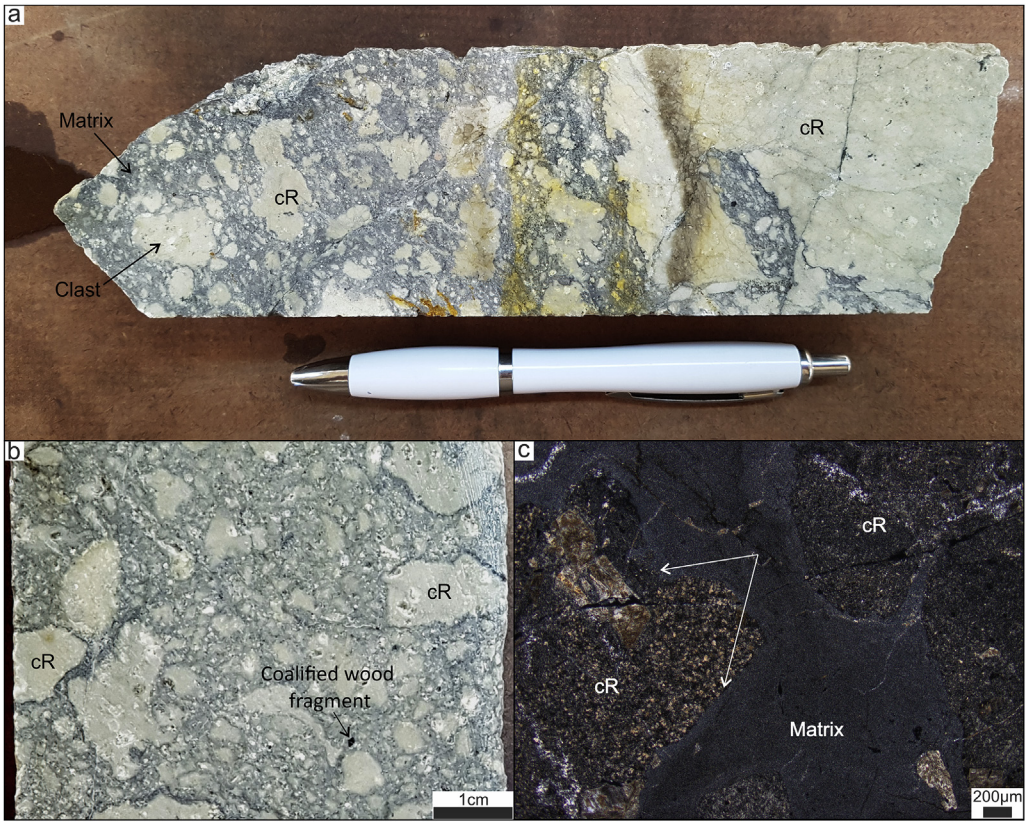

Fig. 6. Matrix-poor monomictic breccias with tuffaceous matrix (mpBx). a) Drill-core sample showing the overall aspect of this breccia. Note the lobate/ragged geometry of most clasts and the presence of some clasts with combined lobate and angular shapes. b) Detailed view of a drill-core sample sowing the presence of coalified wood. c) Photomicrograph under crossed polarized light of cR clasts with combined lobate and planar margins (white arrows) in a vitreous matrix (black).

5.3. Matrix-poor monomictic breccias with tuffaceous matrix (mpBx)

These poorly-sorted matrix-supported breccias are characterized by cR clasts that range from less than a centimeter up to a few decimeters in size (Fig. 6a and b). Most clasts are characterized by irregular shapes with lobate/ragged geometry (Fig. 6b and d); however, clasts with angular geometries and curviplanar margins are also present in lower proportions (Fig. 6a). Clasts showing coexisting irregular and subplanar margins can also be identified (Fig. 6c and d).

Matrix contents range between 15 and 50% in volume and are composed of a mixture of glassy material identical to the clasts (90–95%) and minor amounts of clastic material derived from the pyroclastic sequence hosting the intrusion (10-5%), including coalified wood fragments (Fig. 6a). These breccias form a continuous envelope surrounding the jmBx facies with a thickness ranging between 1 and 50 m and with gradational contacts with the surrounding facies (Figs. 2 and 8).

Interpretation: The monolithological nature of the clasts and the presence of relatively low proportions of a matrix, composed of a mixture of material derived both from the cR facies and the host rocks, support the interpretation of these rocks compact peperites (Hanson and Wilson, 1993; Doyle, 2000; Skilling et al., 2002), formed in the middle portions of the breccia envelope. This type of breccias suggests that the pyroclastic sequence was wet and poorly consolidated at the time of the rhyodacite intrusion (McPhie, 1993).

5.4. Matrix-rich polymictic breccias with tuffaceous matrix (mrBx)

This facies is composed of poorly-sorted matrix-supported breccias (Fig. 7a) with sub-rounded to subangular cR clasts with curviplanar margins (Fig. 7a, b and d) and lithic clasts derived from the pyroclastic host rocks (including ignimbrites and coalified wood fragments, Fig. 7a, c and d). Matrix contents are always greater than 50% in volume and is typically composed of glass shards, small pumice fragments and crystalloclasts (quartz and plagioclase) which are indistinguishable from those in the matrix of the Hydromagmatic Sequence.

As in the previous facies, these breccias form an envelope around the previous facies and constitutes the outermost portion of the brecciated selvage that surrounds the cryptodome contacts with both the mpBx and the Hydromagmatic Sequence are gradational and characterized by size and abundance variations of the cR derived clasts. Also, the passage to the Hydromagmatic Sequence occurs by the sudden appearance of the typical stratification of these rocks after an interval that may vary from a few meters up to tens of meters (Figs. 2 and 8). Inwards, the passage occurs by a progressive decrease in the matrix percentage and by the appearance of clasts with lobate/ragged and mixed geometries (lobate and angular).

Interpretation: Based on the observed transitional contacts, and the nature and abundance of both clasts and matrix, this facies is interpreted as dispersed peperites (Hanson and Wilson, 1993; Doyle, 2000; Skilling et al., 2002), formed in the outer portion of the breccia envelope as the result of the interaction between the rhyodacitic magma and a wet and poorly consolidated pyroclastic sequence.

5.5. Facies architecture

By integrating information obtained from surface outcrops, especially in the southern wall of the Armadillo open-pit, with underground data from diamond drilling holes (Fig. 8a and b respectively), we were able to reconstruct the overall geometry of the intrusion, as well as the distribution and architecture of the facies that compose it. These observations show that the intrusion is a cryptodome characterized by a relatively flat top that forces up part of the Hydromagmatic Sequence, resulting in small folds with wavelengths up to tens of meters (Fig. 8a and b). The data also shows a relatively simple internal structure for the intrusion, with all the described facies distributed in a concentric array (Fig. 8b) and characterized by transitional contacts between them.

The core of the body is represented by the coherent cR facies,

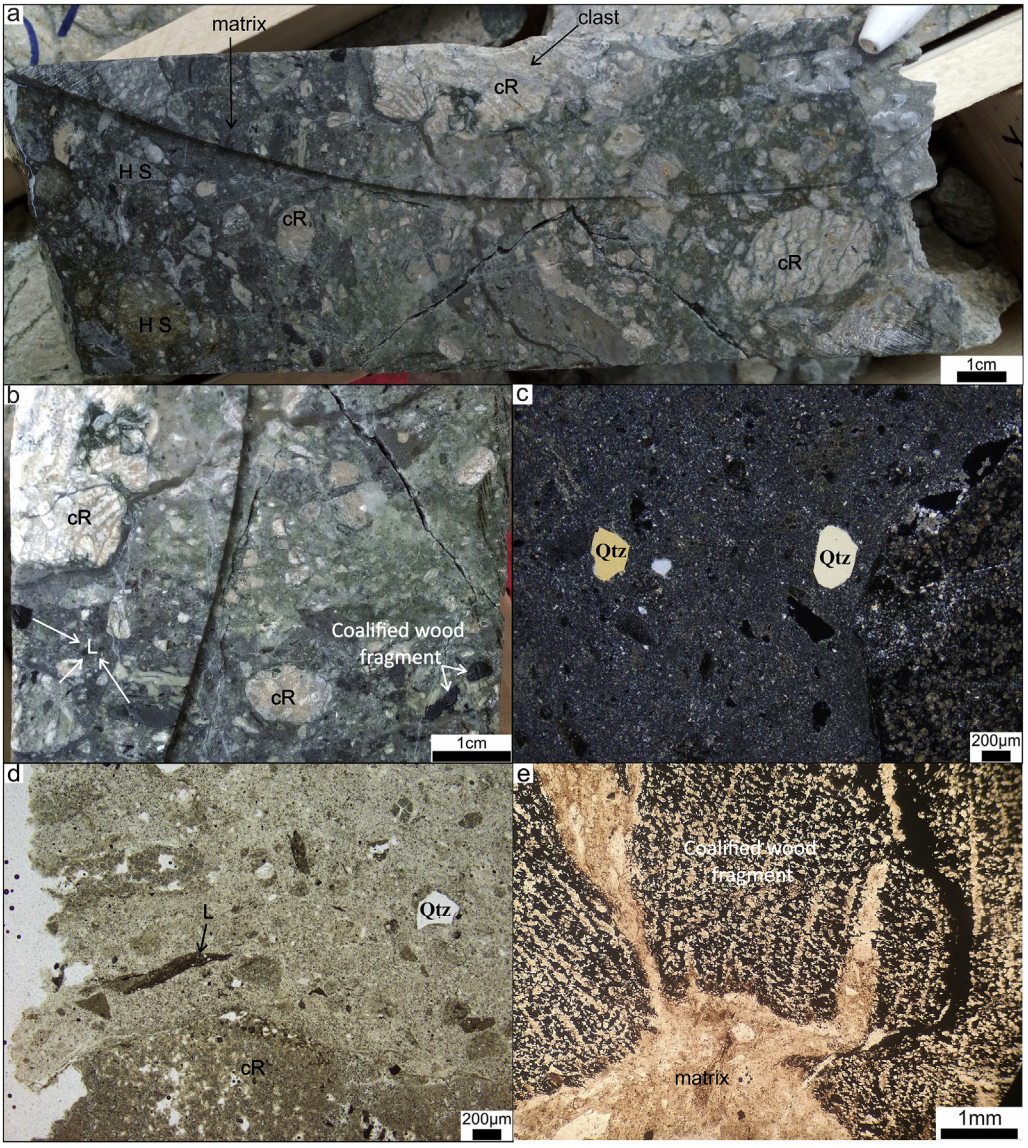

Fig. 7. Matrix-rich polymictic breccias with tuffaceous matrix (mrBx). a) Drill-core sample showing the overall look of this facies, with rhyodacitic lava clasts (cR) and lithoclasts derived from host rocks (L) supported by a fine-grained matrix identical to the pyroclastic host rocks. b) Detail view showing the presence of coalified wood. c, d) Thin section photomicrographs, rhyodacitic lava (cR) and pyroclastic facies lithic clasts (L) and quartz crystalloclasts (Qtz) are supported by a fine-grained matrix. e) Thin section photomicrographs, matrix injected into the spokes of a coalified wood.

characterized by its vitreous nature and the presence of a penetrative magmatic foliation. The brecciated portion of the intrusive constitutes a significant volume of the body, in some places representing more than the 60% of its total thickness (Fig. 2b) and constitutes a continuous envelope with thicknesses between 10 m and 70 m surrounding the coherent interior (Figs. 2b and 8b). This envelope is characterized by an inner zone composed of intrusive hialoclastites (jmBx), a middle zone characterized by close-packed peperites (mpBx), and an external zone dominated by dispersed peperites (mrBx); finally the outermost facies transitions into the pyroclastic rocks that constitute the host rocks of the intrusive (the Hydromagmatic Sequence) by a progressive decrease in the proportion of cR derived clasts and the sudden appearance of stratification surfaces within the host rocks.

6. Discussion

Brecciated envelopes are a common feature in association to the margins of subvolcanic intrusions (Cas and Wright, 1988; McPhie et al., 1993) and have been reported in sills (e.g. McPhie, 1993; Curtis and Riley, 2003; Páez et al., 2018), dikes (e.g. Goto and McPhie, 1996; Kano, 2002; Kwon and Gihm, 2017), laccoliths (e.g. Hanson and Hargrove, 1999; Coira and Pérez, 2002) and cryptodomes (e.g. Stewart and McPhie, 2003; Páez et al., 2018; Burchardt et al., 2019; Goto and Tomiya, 2019) located across several geological environments including sedimentary basins, underwater volcanic environments and subaerial volcanic terranes (Skilling et al., 2002; Van Otterloo et al., 2015; White et al., 2015). The nature of these breccias and the resulting facies arrangement will be strongly dependent on the viscosity of the intruding magmas (e.g. Busby-Spera and White, 1987; Doyle, 2000; Dadd and Van Wagoner, 2002; Skilling et al., 2002), the presence or absence of pore water in the host rocks (e.g. McPhie, 1993; Stewart and McPhie, 2003; Goto and Tomiya, 2019; Németh and Kósik, 2020), the nature of the host rocks (clastic unconsolidated vs. consolidated rocks, e.g. Busby-Spera and White, 1987; McPhie, 1993; Skilling et al., 2002), and the overall intrusion mechanisms (single vs. multipulse intrusion, e.g. Goto and McPhie, 1998; Stewart and McPhie, 2003; Németh et al., 2008; Páez et al., 2018; Goto and Tomiya, 2019). This complex interplay of factors may result in the formation of three distinct breccia

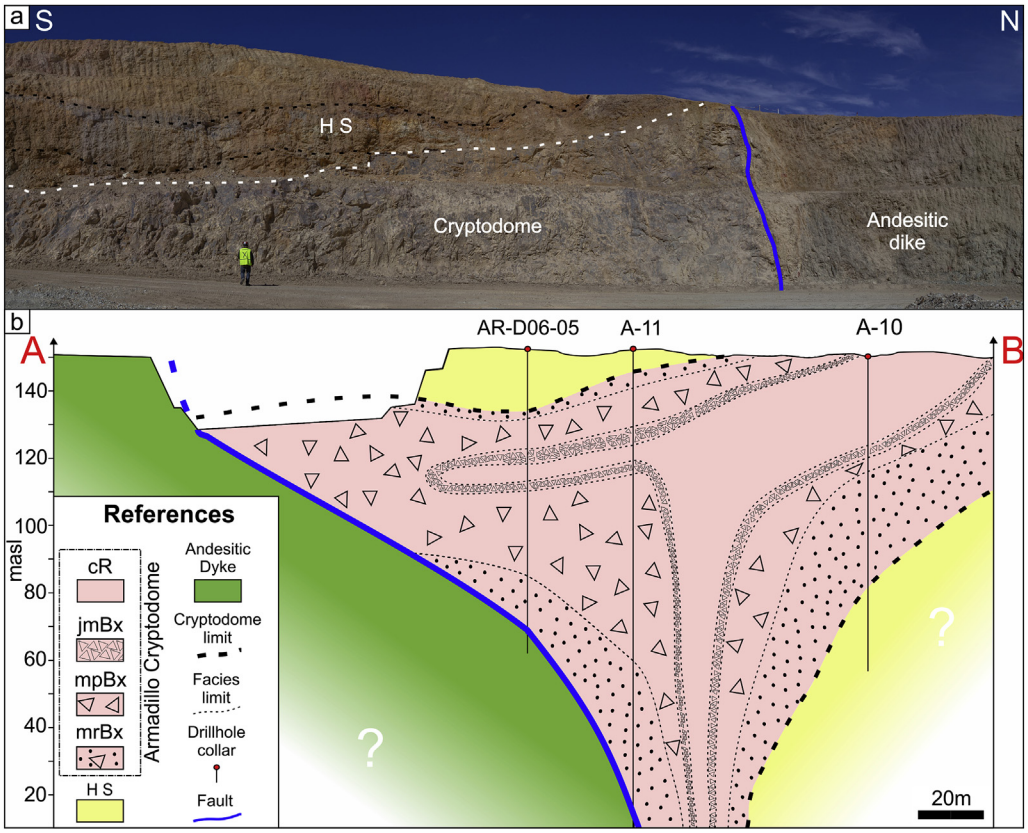

Fig. 8. a) Panoramic view of the Armadillo open-pit southern wall where it is possible to observe the Armadillo Cryptodome intruding and folding the Hydromagmatic Sequence (HS). Also, the tectonic contact with the andesitic dike can also be seen (fault in blue line). b) Geological cross-section showing the overall shape of the Armadillo Cryptodome and the distribution of the facies within it. The apparent low inclination of the fault is the result of the oblique orientation of the profile trace (red line in Fig. 2a) with respect to the fault plane. (For interpretation of the references to color in this figure legend, the reader is referred to the Web version of this article.)

types: autobreccias, hyaloclastites and peperites (Cas and Wright, 1988; McPhie et al., 1993).

When an intrusion occurs into a dry host rock may lead to the formation of autobreccias as the result of mechanical fragmentation of a flowing viscous magma (McPhie et al., 1993); while if pore water is present at the host rocks, intrusive hyaloclastites may develop instead in response to quench fragmentation (Van Otterloo et al., 2015). Therefore, the development of autobreccias vs. hyaloclastites at the margins of an intrusion will largely depend on the predominating fragmentation mechanism (mechanical vs. thermal stress; Cas and Wright, 1988; McPhie et al., 1993; Van Otterloo et al., 2015). However, and despite they form under the influence of very distinct fragmentation mechanisms, the resulting breccias can be sometimes hard to distinguish, especially in older volcanic terranes, as both are monolithological rocks with a jigsaw-fit to rotated internal structure, a variable matrix content and a cast to matrix supported arrangement (Cas and Wright, 1988; McPhie et al., 1993). In those cases, clast geometry, the presence of glassy/altered rims in most clast and/or the development of gradational contacts with peperites, and/or the fracture pattern in the coherent facies may help to correctly identify some of these rocks (Cas and Wright, 1988; McPhie et al., 1993; Van Otterloo et al., 2015; Goto and Tomiya, 2019). In addition to hyaloclastites, peperites can form during intrusion if the host rocks are poorly consolidated and water saturated (Skilling et al., 2002; Van Otterloo et al., 2015; White et al., 2015). These breccias develop in response to clast movement and transportation into a fluidized mixture of juvenile clasts and host sediments as the result of the sudden vaporization (flashing) of the poral water contained in the host rocks during magma intrusion (Kokelaar, 1982; Skilling et al., 2002). Therefore, the predominance of hyaloclastites vs. peperites will mostly depend of the consolidated vs. unconsolidated nature of the clastic host rocks (McPhie et al., 1993; Skilling et al., 2002).

In the following section, the previously described facies and their distribution around the Armadillo cryptodome are used to discuss both the conditions leading to clast fragmentation and transport in the different portions of the breccia envelope, and also to propose an intrusion model based on comparisons with other examples from around the world.

6.1. Clast fragmentation mechanisms

For the Armadillo intrusion, four main juvenile (cR-derived) clast geometries can be identified across the breccia envelope: a) Blocky subangular clasts with sub-planar margins (jmBx facies, Fig. 5a); b) Irregular fluidal-shaped clasts (mpBx facies, Fig. 6a); c) Clasts with coexisting irregular (fluidal) and sub-planar margins (mpBx facies, Fig. 6b and c): and d) Sub-angular to sub-rounded clasts (mrBx facies, Fig. 7a).

The presence of blocky angular to subangular clasts with curviplanar margins in a jigsaw-fit arrangement (Fig. 5a) at the inner portions of the breccia envelope (i.e. hyaloclastites, jmBx facies) implies in-situ non-explosive magma fragmentation due to supercooling in an environment subjected to extreme temperature contrasts (Busby-Spera and White, 1987; McPhie et al., 1993; Van Otterloo et al., 2015; Skilling et al., 2002). Under these conditions, magma is quenched and fragmented by the propagation of tensile cooling cracks produced by thermal stress in response to the influence of an external coolant, such as pore water trapped within the host rocks (McPhie et al., 1993; Van Otterloo et al., 2015). Moreover, the presence of hyaloclastites with matrix-supported textures and up to 20% fine-grained cR derived matrix within this facies suggest intense quench fragmentation occurring at the inner portions of the breccia envelope at the time of the intrusion (Van Otterloo et al., 2015; Páez et al., 2018).

On the other hand, the presence of irregularly shaped fluidal clasts (Fig. 6b) in the central portions of the breccia envelope (i.e. compact peperites, mpBx facies) indicate that they were formed under the ductile regime, suggesting that the development of vapor films may have prevented the direct contact between the molten magma and the poral water, therefore allowing clast deformation in concomitance with

magma fragmentation and transportation within the peperites (Kokelaar, 1982; Busby-Spera and White, 1987; McPhie, 1993; Skilling et al., 2002).

Also at the central parts of the breccia envelope, clasts with coexisting irregular (fluidal) and sub-planar margins (Fig. 6c) suggest a more complex fragmentation history, with changes in the fragmentation mechanism occurring as the magma-wet sediment interaction progresses in time (Goto and McPhie, 1996; Dadd and Van Wagoner, 2002; Martin and Németh, 2007), and therefore indicates that quenching postdates ductile deformation during clast formation. This change was explained by Goto and McPhie (1996) and Doyle (2000), as the result of an increase in magma viscosity in response to magma cooling as fragmentation progressed and vapor films collapse.

Finally, the outer portion of the breccia envelope (i.e. dispersed peperites, mrBx facies) is characterized by sub-angular to sub-rounded clasts with curviplanar margins (Fig. 7a), which are interpreted here as the final product of quench fragmentation completely overprinting the initial fluidal shapes of peperite clasts (Goto and McPhie, 1996; Dadd and Van Wagoner, 2002; Martin and Németh, 2007).

6.2. Clast movement and transportation

When comparing intrusive hyaloclastites and peperites, the main difference is that the first one is generally characterized by little or no clast movement (limited to the immediate edge of the intrusion), and without any mixing between igneous material and the hosting sediments; whereas the latter involves significant clast movement and dispersion within the surrounding unconsolidated clastic host rocks (McPhie et al., 1993; Skilling et al., 2002; Van Otterloo et al., 2015; White et al., 2015). As intrusive hyaloclastites evidence an in-situ fragmentation process (see Van Otterloo et al., 2015 for a full review), clast movement in the inner portions of the Armadillo cryptodome (jmBx facies) is interpreted to be absent, or only limited to a small degree of rotation, but without having suffered any significant transportation.

On the other hand, and for the central and outer breccia envelope (mpBx and mrBx facies), the transportation of juvenile clast during peperite formation is interpreted to be the result of fluidization (see Skilling et al., 2002 for a detailed review of the different transport mechanisms in peperites). This interpretation is supported by the gradational contacts observed between the peperites and the host rocks, and by the destruction of sedimentary structures toward the outer portions of the breccia envelope (e.g. Kokelaar, 1982; McPhie et al., 1993; Goto and McPhie, 1996). Considering that thermally induced fluidization leading to peperite formation is a pressure dependent process, the maximum intrusion depth for the studied cryptodome is estimated to have been less than 1.6 km based on the calculations of Kokelaar (1982). Below this point, the lithostatic pressures usually exceed the critical pressure of water (312 bars for seawater, Kokelaar, 1982), greatly inhibiting the sudden volume expansion of the heated poral water, which in turn hinders fluidization.

6.3. Emplacement conditions and timing between the formation of breccias

The widespread presence of hyaloclastites and peperites, which form a selvage of several tens of meters around the coherent facies of the Armadillo cryptodome (Figs. 2b and 8b) evidence: 1) the water saturated state and the low degree of consolidation of the Hydromagmatic Sequence at the time of the intrusion (Skilling et al., 2002; Van Otterloo et al., 2015; White et al., 2015) and 2) demonstrates a relative contemporaneity of the rhyodacitc magmas and the hydromagmatic sequence that host the intrusion (e.g. Hanson and Schweickert, 1982; Einsele, 1986; Kano, 1989; Maas, 1992; Summer and Ayalon, 1995).

Previous works show that the development fluidal clasts in peperites is controlled by both the magma viscosity and the grain size of the hosting sediments, when considering the same host rocks, lower viscosity magmas tend to favor the development of fluidal clasts, whereas higher viscosity magmas tend to develop angular to blocky clasts (Busby-Spera and White, 1987; Doyle, 2000; Dadd and Van Wagoner, 2002; Skilling et al., 2002; Martin and Németh, 2007), so the presence of fluidal clasts can be used as indicative of relatively low viscosities for the rhyodacitic magmas of the Armadillo intrusion.

Despite most examples of fluidal peperites involve mafic to intermediate magmas (Skilling et al., 2002), several examples of felsic fluidal examples are also known (e.g. Ramsey Island in Wales, Kokelaar, 1982; Sierra Nevada, USA, Hanson, 1991; Tennant Creek in Australia, McPhie, 1993). Most of these studies explain this problem by suggesting that magma viscosities are much lower than those typically expected for these compositions, conditions that can be achieved due to the fact that viscosity of silicic magmas declines when the temperature, volatile content and confining pressure are all high (Kokelaar, 1982; Hanson, 1991; McPhie, 1993; Skilling et al., 2002; Goto and Tsuchiya, 2004), or also as a consequence of high concentrations of components that could cause magma depolymerization, such as alkalis or halogens (Skilling et al., 2002). As the Armadillo cryptodome is composed of subalkaline rhyodacites (Fig. 4e) depolymerization can be ruled out, and therefore lower magma viscosities can be most likely interpreted as the result of a combination of factors including: 1) the low phenocryst contents (typically below 10–15%) and the glassy groundmass (with few microlites) of the coherent facies may suggests that the magma had a high (near-liquidus) temperature at the time of the intrusion; and 2) the complete absence of vesicles in the coherent facies could also suggest that volatiles may have remained in solution within the melt due to the weight of the Hydromagmatic Sequence overlying the intrusion (over 120 m in thickness). Finally, Martin and Németh (2007) suggested that peperite clast geometry may also be influenced by the emplacement rates of the magma, with lower emplacement rates favoring fluidal clast development.

Considering the previous discussion, a slow inflation of the cryptodome, combined with the lower viscosities interpreted for the magmas, may account for explaining the fluidal clasts recognized in the peperites and can be further used to discuss the emplacement mechanism of the Armadillo cryptodome (Fig. 9). The simple geometry and concentric arrangement of facies described for this cryptodome (Fig. 8b), its flow-banded interior (cR facies), the transitional contacts between them and the upward forced strata atop of the intrusion (Fig. 8a), all suggest that this body most likely formed from a single intrusive pulse due to the steady injection of magma in a relatively continuous episode (Fig. 9a), in a similar way as the Rebun Island intrusive (Goto and McPhie, 1998), the Milos Island cryptodome (Stewart and McPhie, 2003), the Tate-iwa dome (Goto and Tsuchiya, 2004) or the El Guanaco cryptodomes (Páez et al., 2018). This concentric arrangement of facies is also consistent with an endogenous inflation model, where new magma is added in the cryptodome interior (Cas and Wright, 1988; Sigurdsson, 2015).

As the cryptodome inflation progressed (Fig. 9b), flow-banding developed in the coherent interior (cR facies) in response to laminar shear during the addition of new lava (Cas and Wright, 1988; Sigurdsson, 2015). At the same time, in the outer rim of the intrusion, the interplay of magma flow and fluidization of the host rocks resulted in the development of a fluidal peperite envelope (Fig. 9b). At this point quench fragmentation was most likely inhibited by the development of stable vapor films, preventing the direct contact between magma and the poral water, and allowing the development of the fluidal clasts observed in this breccias (mpBx facies), in a similar way to other fluidal peperites (e.g. Busby-Spera and White, 1987; Martin and Németh, 2007; Páez et al., 2018).

Clast geometries at the Armadillo peperites suggest that quench fragmentation was limited mostly to the end of the brecciation process (Fig. 9c), when the insulating vapor films collapsed, allowing water to enter in direct contact with the fluidal magma clasts (Van Otterloo et al., 2015). This resulted in mixed clast geometries and clasts with

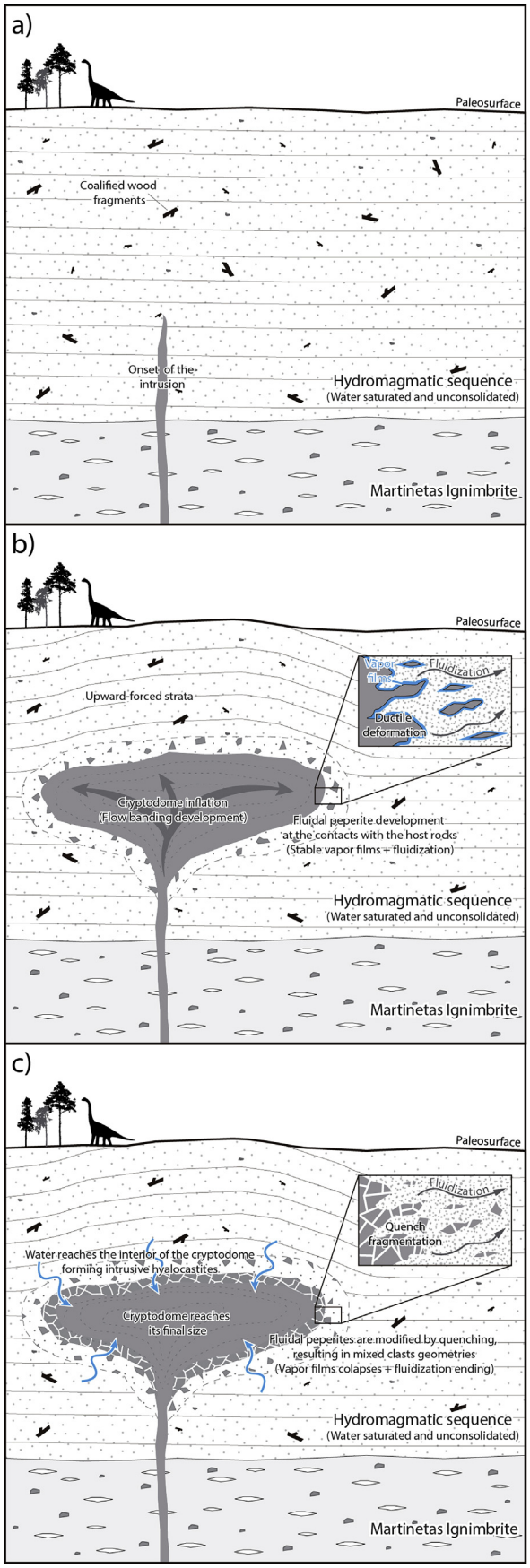

Fig. 9. Emplacement model of the Armadillo Cryptodome a) The onset of the intrusion occurred as a the rhyodacitic magma reached the water saturated and poorly consolidated Hydromagmatic sequence. b) The cryptodome underwent a relatively steady endogenous inflation stage resulting in a flow-banded core. At this stage, the development of stable vapor films insulating the flowing magma and the widespread fluidization of the host rocks resulted in an envelope of fluidal peperites surrounding the inflating body. c) After the end of the inflation stage, the collapse of vapor films resulted in quench fragmentation modifying the originally fluidal shape of many clast at the peperites. At the same time water invaded the inner portions of the intrusion, causing widespread quenching and the development of intrusive hyaloclastites at the edges of the coherent facies. See the text for further information.

coexisting fluidal and sub-planar margins in the central and outer portions of the breccia envelope (mpBx and mrBx facies), a common occurrence in several peperites undergoing this process (e.g. Hanson and Hargrove, 1999; Martin and Németh, 2007; Vezzoli et al., 2009; Páez et al., 2018).

At this point, water probably also invaded the inner portions of the intrusion (Fig. 9c), resulting in widespread development of hyaloclastites at the edges of the coherent facies (jmBx facies). Here, quench fragmentation is also interpreted to have postdated the main inflation phase of the intrusion, as the hyaloclastites are composed exclusively of jigsaw-fit flow-banded clasts where the continuity of flow-banding across them implies no relative movement between clasts after its formation (Fig. 5a). This interpretation is also supported by the absence of lobes/fingers of coherent rhyodacite (cR facies) intruding or cross-cutting the hyaloclastites. In this regard, the progressive increase in matrix contents and the diminishing clast sizes observed toward the outer portions of this facies, are interpreted as the result of an increase in the fragmentation intensity toward the outside of the intrusion, where the thermal gradients are interpreted to be at its highest due to the higher availability of water (McPhie et al., 1993; Van Otterloo et al., 2015; White et al., 2015).

Finally, it is important to note that, despite brecciation processes are described here as a continuous and lineal succession of events, occurring simultaneously along the entire breccia envelope; the authors consider that the most likely scenario is that they occurred at different scales, times and intensities at different positions within the breccia envelope as the intrusion progressed.

7. Summary and conclusions

This work includes the first detailed facies description of an intrusive body defined as a cryptodome for the Deseado Massif, a region of the Argentinian Patagonia characterized by widespread Jurassic volcanism and Au–Ag epithermal mineralization. Its relatively simple geometry and access to mining infrastructure and information (Open pits, drill cores, maps, etc.) represent a unique opportunity to study the interaction of felsic magmas with poorly consolidated and water saturated pyroclastic rocks.

Facies analysis allowed us to infer this body as the result of a low viscosity rhyodacitic magma intruding at a depth ranging between 0,12 and 1,6 km, enough to suppress volatile separation of the magma but not too deep to inhibit the fluidization of the host rocks. The intrusion is interpreted to have occurred in a single and steady endogenous inflation pulse, resulting in the development of a flow banded core and a fluidal peperite envelope due to the combination of relatively low magma viscosities (for a rhyodacitic melt), the development of stable vapor films insulating the flowing magma and allowing the ductile deformation of the rhyodacite clasts, and the fluidization of the unconsolidated and water saturated host rocks. During this stage, the overlying pyroclastic sequence was also deformed (upward-forced) as the cryptodome grew.

After the inflation stage stopped, the collapse of the vapor films resulted in quench fragmentation modifying the originally fluidal shape

of many clasts at the peperites, especially at the outer portion of the breccia envelope where fluidal clast shapes were almost completely erased due to this process. At the same time water invaded the inner portions of the intrusion, causing widespread quenching and the development of intrusive hyaloclastites at the edges of the coherent facies, crosscutting the flow banding of the rhyodacite.

Finally, and although the intrusion of magmas into wet sediments may give rise to significant hydrothermal systems (McPhie, 1993; Cathles et al.,1997; McPhie and Orth, 1999; Skilling et al., 2002), and thus lead to substantial hydrothermal alteration and/or mineralization (e.g. Sillitoe and Bonham, 1984; Cas, 1992; Boulter, 1993; Wallace et al., 2003; Gifkins et al., 2005; Popkhadze and Moritz, 2014A), the lack of detailed geochronological studies at the Don Nicolas Mine precludes us to directly link the studied intrusion with the gold-bearing mineralization found at mine. Still, the presence of widespread intrusive hyaloclastite and peperites prove that water saturation conditions may have prevailed in the pyroclastic sequence for a significant amount of time. This could be of importance for explaining the presence of an economic grade mineral deposit, as mixing between meteoric (c.f. cognate) and magmatic waters is considered an important process for epithermal mineralization to develop (see Hedenquist et al., 2000; Simmons et al., 2005).

CRediT authorship contribution statement

FacundoJ.De Martino: Conceptualization, Methodology, Investigation, Software, Resources, Project administration, Writing - original draft. **GerardoN. Paez:** Conceptualization, Methodology, Investigation, Software, Funding acquisition, Writing - original draft. **HoracioJ. Echeveste:** Visualization, Funding acquisition, Validation, Writing - review & editing. **SebastiánM. Jovic:** Validation, Writing - review & editing. **Mario O.R. Tessone:** Validation, Writing - review & editing.

Declaration of competing interest

The authors declare that they have no known competing financial interests or personal relationships that could have appeared to influence the work reported in this paper.

Acknowledgements

This research is part of F.J. De Martino PhD thesis and was funded through a CONICET PhD grant, the generous logistical support of Minera Don Nicolás S.A. and additional funds from the UNLP Grant N892 entitled “Estudio de complejos de domos félsicos asociados a sistemas hidrotermales” (Universidad Nacional de La Plata) and the UNLP Grant N797 entitled “Controles volcánico y tectónico de mineralizaciones epitermales jurásicas del Macizo del Deseado”. The authors want to give a special thanks to Silvio Franco and the mine's exploration team for providing access to information and drill-cores, for their valuable discussions and input on the local geology and also for encouraging the publication of this work. Last, but not least, the authors wish to express gratitude to Károly Németh, César Navarrete and the Editor of the JSAES, Andrés Folguera for their help and constructive suggestions that significantly improved the manuscript.

References

Avery, M.R., Panter, K.S., Gorsevski, P.V., 2017. Distinguishing styles of explosive eruptions at Erebus, Redoubt and Taupo volcanoes using multivariate analysis of ash morphometrics. Journal of Volcanology and Geothermal Research 332, 1–13.

Boulter, C.A., 1993. High-level peperitic sills at Rio Tinto, Spain: implications for stratigraphy and mineralization. Trans. Inst. Min. Metall. 102, B30–B38.

Burchardt, S., Mattsson, T., Palma, J.O., Galland, O., Almqvist, B., Mair, K., Jerram, D.A., Hammer, Ø., Sun, Y., 2019. Progressive growth of the Cerro bayo cryptodome, chachahuén volcano, Argentina—implications for viscous magma emplacement. J. Geophys. Res. Solid Earth 124, 2019JB017543. https://doi.org/10.1029/2019JB017543.

Busby-Spera, c.J., White, j.D.L., 1987. Variation in peperite textures associated with differing host-sediment properties. Bull. Volcanol. 49, 765–775.

Cas, R.A.F., 1992. Submarine volcanism: eruption styles, products, and relevance to understanding the host rock successions to volcanic-hosted massive sulfide deposits. ECONOMIC GEOLOGY 87, 511–541.

Cas, R.A.F., Wright, J.V., 1988. Volcanic Successions, Modern and Ancient: a Geological Approach to Processes, Products, and Successions. Allen and Unwin, London, pp. 528p.

Coira, B., Pérez, B., 2002. Peperitic textures of Ordovician dacitic synsedimentary intrusions in Argentina's Puna Highland: clues to emplacement conditions. In: In: Skilling, I.P., White, J.D.L., McPhie, J. (Eds.), Peperite: Processes and Products of Magma-Sediment Mingling, vol. 114. J. Volcanol. Geotherm. Res., pp. 165–180.

Cole, R.P., White, J.D.L., Townsend, D.B., Leonard, G.S., Conway, C.E., 2020. Glaciovolcanic emplacement of an intermediate hydroclastic breccia-lobe complex during the penultimate glacial period (190 − 130 ka), Ruapehu volcano, New Zealand. GSA Bull 1–11. https://doi.org/10.1130/B35297.1.

Curtis, M.L., Riley, T.R., 2003. Mobilization of fluidized sediment during sill emplacement, western Dronning Maud Land, East Antarctica. Antarct. Sci. 15, 393–398. https://doi.org/10.1017/S0954102003001408.

Dadd, K., Van Wagoner, N., 2002. Magma composition and viscosity as controls on peperite texture: an example from Passamaquoddy Bay, southeastern Canada. Journal of Volcanology and Geothermal Research - J VOLCANOL GEOTHERM RES. 114, 63–80. https://doi.org/10.1016/S0377-0273(01)00288-8.

De Giusto, J.M., Di Persia, C.A., Pezzi, E., 1980. Nesocratón del Deseado. In: In: En Turner, J.C. (Ed.), Segundo Simposio de Geología Regional Argentina, vol. 2. Academia Nacional de Ciencias, Córdoba, pp. 1389–1430.

De Martino, F.J., echeveste, h.J., Jovic, S.M., tessone, m.O., 2017. Estratigrafía volcánica bimodal de los proyectos Martinetas y Microondas, sector oriental del Macizo del Deseado, Santa Cruz, Argentina. XX Congreso Geológico Argentino, Actas ST9, pp. 34–38.

De Martino, F.J., Echeveste, H.J., Jovic, S.M., Tessone, M.O.R., Ruiz, R., De Barrio, R.E., Franco, S., 2018. Evolution of mineralizing events in the armadillo vein epithermal system, Martinetas district, eastern Deseado Massif, Santa Cruz, Argentina. 15th Quadrennial IAGOD Symposium. Symposium Proceedings, A- 11, 31–32.

De Martino, F.J., Jovic, S.M., Echeveste, H.J., Tessone, M.O.R., Palma, D.S., 2020. Precipitación de Au vinculada a materia orgánica. Sistema vetiforme armadillo, mina Don Nicolás, Macizo del Deseado. Revista de la Asociación Geológica Argentina 77, 2. (in press). http://ppct.caicyt.gov.ar/index.php/raga/article/view/16835/45454575769720.

De Rita, D., Giordano, G., Esposito, A., Fabbri, M., Rodani, S., 2002. Large volume phreatomagmatic ignimbrites from the colli albani volcano (middle pleistocene, Italy). Journal of Volcanology and Geothermal Research 118 (1–2), 77–98.

Doyle, M.G., 2000. Clast shape and textural associations in peperite as a guide to hydromagmatic interactions: Upper Permian basaltic and basaltic andesite examples from Kiama, Australia. Aust. J. Earth Sci. 47, 167–177.

Echavarría, l.E., Schalamuk, I.B.a., Etcheverry, R.O., 2005. Geologic and tectonic setting of Deseado Massif epithermal deposits, Argentina, based on El Dorado-Monserrat. Journal of South American Earth Sciences 19, 415–432.

Einsele, G., 1986. Interaction between sediments and basalt injectionsin young Gulf of California-type spreading centers. GeologischeRundschau 75, 197–208.

Féraud, G., Alric, V., Fornari, M., Bertrand, H., Haller, M., 1999. 40Ar/39Ar dating of the Jurassic silicic volcanic Province of Patagonia and its relationship to Gondwana breakup and subduction. Earth Planet. Sci. Lett. 172 (1), 83–96.

Fernandez, R.R., Blesa, A., Moreira, P., Echeveste, H., Mykietiuk, K., Andrada De Palomera, P., Tessone, M., 2008. Los depósitos de oro y plata vinculados al magmatismo jurásico de la Patagonia: revisión y perspectivas para la exploración. Revista de la Asociación Geológica Argentina 63 (4), 665–681.

Feruglio, E., 1949. Descripción geológica de la Patagonia. Dirección General de Yacimientos Petrolíferos Fiscales, Tomo II. pp. 349 (Buenos Aires).

Gifkins, C., Herrmann, W., Large, R., 2005. Altered Volcanic Rocks. A Guide to Description and Interpretation. University of Tasmania, Hobart, CODES.

Goto, Y., Tomiya, A., 2019. Internal structures and growth style of a quaternary subaerial rhyodacite cryptodome at ogariyama, usu volcano, hokkaido, Japan. Frontiers in Earth Science 7, 66. https://doi.org/10.3389/feart.2019.00066.

Goto, Y., Tsuchiya, N., 2004. Morphology and growth style of a Miocene submarine dacite lava dome at Atsumi, northeast Japan. Journal of Volcanology and Geothermal Research 134, 255–275.

Goto, Y., McPhie, J., 1998. Endogenous growth of a miocene submarine dacite cryptodome, Rebun island, hokkaido, Japan. J. Volcanol. Geotherm. Res. 84, 273–286.

Goto, Y., McPhie, J., 1996. A Miocene basanite peperitic dyke at Stanley, northwestern Tasmania, Australia. J. Volcanol. Geotherm. Res. 74, 11–120.

Goto, Y., Ito, Y., Yokoyama, Y., Matsui, T., Mimatsu, S., 2004. Internal structure of a subaerial dacite cryptodome at Usu volcano, Hokkaido, Japan. Mem. Muroran Inst. Tech. 54, 3–10.

Guido, D.M., 2004. Subdivisión litofacial e interpretación del volcanismo jurásico (Grupo Bahía Laura) en el este del Macizo del Deseado, provincia de Santa Cruz. Rev. Asoc. Geol. Argent. 59 (4), 727–742.

Guido, D., Campbell, K., 2011. Jurassic hot spring deposits of the Deseado Massif (Patagonia, Argentina): characteristics and controls on regional distribution. Fuel and Energy Abstracts 203, 35–47. https://doi.org/10.1016/j.jvolgeores.2011.04.001.

Guido, D., Schalamuk, I., 2003. Genesis and exploration potential of epithermal deposits from the Deseado Massif, argentinean Patagonia. In: In: Eliopoulos (Ed.), Mineral Exploration and Sustainable Development, vol. I. Balkema, Rotterdam, pp. 493–496.

Hanson, R.E., 1991. Quenching and hydroclastic disruption of andesiticto

rhyoliticintrusions in a submarine island-arc sequence, northern Sierra Nevada, California. Geol. Soc. Am. Bull. 103, 804–816.
Hanson, R.E., Schweickert, R.A., 1982. Chilling and brecciation of a Devonian rhyolitic sill intruded into wet sediments, northern Sierra Nevada, California. J. Geol. 90, 717–724.
Hanson, R.E., Wilson, T.J., 1993. Large-scale rhyolitic peperitas (Jurassic, southern Chile). J. Volcanol. Geotherm. Res. 54, 247–264.
Hanson, R.E., Hargrove, U.S., 1999. Processes of magma/wet sediment interaction in a large-scale Jurassic andesitic peperite complex, northern Sierra Nevada, California. Bull. Volcanol. 60, 610–626. https://doi.org/10.1007/s004450050255.
Hedenquist, J.W., Arribas Jr., A., Urien-Gonzalez, E., 2000. Exploration for epithermal gold deposits. In: In: Hagemann, S.G., Brown, P.E. (Eds.), Gold in 2000: Society of Economic Geologists, Reviews in Economic Geology, vol. 13. pp. 245–277.
Kano, K.I., 1989. Interactions between andesitic magma and poorly consolidated sediments: examples in the Neogene Shirahama Group, South Izu, Japan. J. Volcanol. Geotherm. Res. 37, 59–75.
Kano, K., 2002. Middle Miocene volcaniclastic dikes at Kukedo, Shimane Peninsula, SW Japan: fluidization of volcaniclastic beds by emplacement of syn-volcanic andesitic dikes. J. Volcanol. Geotherm. Res. https://doi.org/10.1016/S0377-0273(01)00283-9.
Kay, S.M., Ramos, V.A., Mpodozis, C., Sruoga, P., 1989. Late paleozoic to jurassic silicic magmatism at the Gondwana margin: analogy to the middle proterozoic in north America? Geology 17, 324–328.
Kokelaar, B.P., 1982. Fluidization of wet sediments during the emplacement and cooling of various igneous bodies. J. Geol. Soc. London 139, 21–33.
Kwon, C.W., Gihm, Y.S., 2017. Fluidization of host sediments and its impacts on peperites-forming processes, the Cretaceous Buan Volcanics, Korea. J. Volcanol. Geotherm. Res. https://doi.org/10.1016/j.jvolgeores.2017.05.019.
Llambías, E.J., 2008. Geología de los cuerpos ígneos. Asociación Geológica Argentina, Serie B, Didáctica y Complementaria No. 29, Instituto Superior de Correlación Geológica, Serie Correlación Geológica, vol. 15. pp. 222 (Buenos Aires).
Lovecchio, J.P., Rohais, S., Joseph, P., Bolatti, N.D., Ramos, V.A., 2020. Mesozoic rifting evolution of SW Gondwana: a poly-phased, subduction-related, extensional history responsible for basin formation along the Argentinean Atlantic margin. Earth-Science Rev. 103138. https://doi.org/10.1016/j.earscirev.2020.103138.
Maas, R., 1992. Peperite im Unterkarbon der Südvogesen. Jahrbuch Der Geologische Landesamt Baden-Württemberg 34, 213–237.
Martin, U., Németh, K., 2007. Blocky versus fluidal peperite textures developed in volcanic conduits, vents and crater lakes of phreatomagmatic volcanoes in Mio/Pliocene volcanic fields of Western Hungary. Journal of Volcanology and Geothermal Research 159, 164–178.
McPhie, J., 1993. The tennant Creek porphyry revisited: a synsedimentary sill with peperite margins, early proterozoic, northern territory. Aust. J. Earth Sci. 40, 545–558.
McPhie, J., Orth, K., 1999. Peperite, pumice and perlite in submarine volcanic successions: implications for VHMS mineralization. Proceedings of Pacrim '99, 643–648 Bali, Indonesia.
McPhie, J., Doyle, M., Allen, R., 1993. Volcanic Textures. Centre for Ore Deposit and Exploration Studies, Univ., Tasmania, Hobart, pp. 57–58.
Navarrete, C., Gianni, G., Encinas, A., Márquez, M., Kamerbeek, Y., Valle, M., Folguera, A., 2019. Triassic to Middle Jurassic geodynamic evolution of southwestern Gondwana: from a large flat-slab to mantle plume suction in a rollback subduction setting. Earth-Science Reviews. https://doi.org/10.1016/j.earscirev.2019.05.002.
Németh, K., Pecskay, Z., Martin, U., Gmeling, K., Molnar, F., Cronin, S.J., 2008. Hyaloclastites, peperites and soft-sediment deformation textures of a shallow subaqueous Miocene rhyolitic dome-cryptodome complex, Palhaza, Hungary. Geol. Soc. Lond., Spec. Publ. 302 (1), 63–86.
Németh, K., Kósik, S., 2020. Review of explosive hydrovolcanism. Geosciences 10, 44. https://doi.org/10.3390/geosciences10020044.
Páez, G.N., Permuy Vidal, C., Galina, M., López, L., Jovic, S.M., Guido, D.M., 2018. Intrusive hyaloclastite and peperitic breccias associated to sill and cryptodome emplacement on an Early Paleocene polymagmatic compound cone-dome volcanic complex from El Guanaco mine, Northern Chile. Journal of Volcanology and Geothermal Research; Año 354, 153–170 2018.
Páez, G., Ruiz, R., Guido, D., Rios, F., Subias, I., Recio, C., Schalamuk, I., 2016. High-grade ore shoots at the Martha epithermal vein system, Deseado Massif, Argentina: the interplay of tectonic, hydrothermal and supergene processes in ore genesis. Ore Geology Reviews 72, 546–561. https://doi.org/10.1016/j.oregeorev.2015.07.026.
Pankhurst, R.J., Rapela, C.W., 1995. Production of jurassic rhyolite by anatexis of the lower crust of Patagonia. Earth Planet. Sci. Lett. 134, 23–36. https://doi.org/10.1016/0012-821X(95)00103-J.
Pankhurst, R., Rapela, C., Márquez, M., 1993. Geocronología y petrogénesis de los granitoides Jurásicos del noroeste del Macizo del Deseado. In: 12° Congreso Geológico Argentina, vol. 4. Actas, pp. 134–141.
Pankhurst, R., Leat, P., Sruoga, P., Rapela, C., Márquez, M., Storey, B., Riley, T., 1998. The Chon Aike province of Patagonia and related rocks in West Antarctica: a silicic large igneous province. J. Volcanol. Geotherm. Res. 81, 113–136. https://doi.org/10.1016/S0377-0273(97)00070-X.
Panza, J.L., Haller, M.J., 2002. El volcanismo jurásico. In: Haller, M.J. (Ed.), Geología y recursos Naturales de Santa Cruz. Relatorio del XV Congreso Geológico Argentino, pp. 89–102.
Permuy Vidal, C., Guido, D.M., Jovic, S., Bodnar, R., Moncada, D., Melgarejo, J., Hames, W., 2016. The Marianas-San Marcos vein system: characteristics of a shallow low sulfidation epithermal Au–Ag deposit in the Cerro Negro district, Deseado Massif, Patagonia, Argentina. Mineralium Deposita 51. https://doi.org/10.1007/s00126-015-0633-9.
Popkhadze, N., Moritz, R., 2014A. The Products of Phreatomagmatic Eruption at the Madneuli Polymetallic Deposit, Lesser Caucasus, Georgia. 3th International Course on Collapse Calderas and 5th International Workshop on Collapse Calderas. Taupo, New Zealand, pp. 54 Abstract volume.
Popkhadze, N., Moritz, R., Gugushvili, V., 2014B. Architecture of upper cretaceous rhyodacitic hyaloclastite at the polymetallic madneuli deposit, lesser caucasus, Georgia. Open Geosci 6https://doi.org/10.2478/s13533-012-0182-z(PDF) Evidence of shallow-marine depositional environment of the host. rocks of the Madneuli polymetallic deposit, Bolnisi district, Lesser Caucasus, Georgia. Available from: , Accessed date: 19 February 2020. https://www.researchgate.net/publication/299738109_Evidence_of_shallow-marine_depositional_environment_of_the_host_rocks_of_the_Madneuli_polymetallic_deposit_Bolnisi_district_Lesser_Caucasus_Georgia.
Rapela, C.W., Kay, S.M., 1988. Late Paleozoic to recent magmatic evolution of northern Patagonia. Episodes 11 (3), 175–182.
Riley, T.R., Flowerdew, M.J., Pankhurst, R.J., Curtis, M.L., Millar, I.L., Fanning, C.M., Whitehouse, M.J., 2017. Early jurassic magmatism on the antarctic Peninsula and potential correlation with the subcordilleran plutonic belt of Patagonia. J. Geol. Soc. London. 174, 365–376. https://doi.org/10.1144/jgs2016-053.
Rissmann, C., Nicol, A., Cole, J., Kennedy, B., Fairley, J., Christenson, B., Leybourne, M., Milicich, S., Ring, U., Gravley, D., 2011. Fluid flow associated with silicic lava domes and faults, Ohaaki hydrothermal field, New Zealand. J. Volcanol. Geotherm. Res. 204, 12–26. https://doi.org/10.1016/j.jvolgeores.2011.05.002RITTMANN, A. 1962. Volcanoes and their Activity. Inter-science, New York, 305 pp. (Translated from Rittmann, A., 1960. Vulkane und ihre Tätigkeit. Ferdinand Enke, Stuttgart.).
Rocchi, S., Breitkreuz, C., 2017. Physical geology of shallow-level magmatic systems - an introduction. In: Advs in Volcanology, pp. 1–10. https://doi.org/10.1007/11157_2017_32.SAKAMOTO, I. 1998. Morphological features and petrographical changes between hyaloclastite to peperite of Membo rhyolite lava, observed around Senryoike inlet, Kozu-shima Is., Japan. IAVCEI Int. Volcanol. Congress, Cape Town, Abstracts, 51.
Schalamuk, I., Zubia, M., Genini, A., Fernández, R., 1997. Jurassic epithermal Au-Ag deposits of Patagonia, Argentina. Ore Geol. Rev. 12 (3), 173–186.
Schalamuk, I.B., Guido, D., de Barrio, R.E., Fernández, Y.R.R., 1999. Hot spring structures from el macanudo-el mirasol area, Deseado Massif, Argentina. In: Stanley, Schalamuk, Guido, de Barrio y Fern·ndez (Eds.), Mineral Deposits Processes to Processsing, pp. 577–580.
Schmiedel, T., Galland, O., Breitkreuz, C., 2017. Dynamics of sill and laccolith emplacement in the brittle crust: role of host rock strength and deformation mode. J. Geophys. Res. Solid Earth 122, 8860–8871. https://doi.org/10.1002/2017JB014468SECRETARÍA DE POLÍTICA MINERA. 2019.
Secretaría de Política Minera, 2019. Catastro Minero Unificado [online]. Available from: http://cima.minem.gob.ar/dataset/2100/catastro-minero-unificado, Accessed date: 20 November 2019.
Self, S., 1983. Large-scale phreatomagmatic silicic volcanism; a case study from New Zealand. Journal of Volcanology and Geothermal Research 17 (1–4), 433–469.
Sheridan, M.F., Wohletz, K.H., 1983. Hydrovolcanism: basic considerations and review. J. Volcanol. Geotherm. Res. 17, 1–29.
Sigurdsson, H., 2015. The Encyclopedia of Volcanoes, second ed. Elsevier, London, England, pp. 1456.
Skilling, I.P., White, J.D.L., McPhie, J., 2002. Peperite: a review of magma-sediment mingling. Journal of Volcanology and Geothermal Research 114, 1–17.
Sillitoe, R.H., 2018. Why No porphyry copper deposits in Japan and South Korea? Resource Geology 68 (2), 107–125. https://doi.org/10.1111/rge.12156.
Sillitoe, R.H., Bonham, H.F., 1984. Volcanic landforms and ore deposits Econ. Geol 79, 1286–1298 1984.
Simmons, S.F., White, N.C., John, D.A., 2005. Geological characteristics of epithermal precious and base metal deposits. Economic Geology 100th Anniversary Volume 485–522.
Stewart, A.L., McPhie, J., 2003. Internal structure and emplacement of an upper pliocene dacite cryptodome, Milos island, Greece. Journal of Volcanology and Geothermal Research 124, 129–148.
Storey, B.C., Kyle, P.R., 1997. An active mantle mechanism for Gondwana breakup. S. Afr. J. Geol. 100 (4), 283–290.
Storey, B.C., Alabaster, T., Pankhurst, R.J., 1992. Magmatism and the Causes of Continental Break-Up, vol. 68. Geological Society of London Special Publications, pp. 404.
Storey, B., Vaughan, A., Riley, T., 2013. The links between large igneous provinces, continental break-up and environmental change: evidence reviewed from Antarctica. Earth and Environmental Science Transactions of the Royal Society of Edinburgh 104, 17–30. https://doi.org/10.1017/S175569101300011X.
Summer, N.S., Ayalon, A., 1995. Dike intrusion into unconsolidated sandstone and the development of quartzite contact zones. Journal of Structural Geology 17, 997–1010.
Van Otterloo, J., Cas, R.A.F., Scutter, C.R., 2015. The fracture behaviour of volcanic glass and relevance to quench fragmentation during formation of hyaloclastite and phreatomagmatism. Earth Sci. Rev. 151, 79–116.
Vezzoli, L., Matteini, M., Hauser, N., Omarini, R., Mazzuoli, R., Acocella, V., 2009. Non-explosive magma–water interaction in a continental setting: miocene examples from the Eastern Cordillera (central Andes; NW Argentina). Bull. Volcanol. 71, 509–532. https://doi.org/10.1007/s00445-008-0239-5.
Wallace, P.J., De Vivo, Benedetto, Bodnar, Robert J., 2003. From mantle to atmosphere: magma degassing, explosive eruptions, and volcanic volatile budgets. In: Developments in Volcanology, vol. 5. Elsevier, pp. 105–127. https://doi.org/10.1016/S1871-644X(03)80026-8.
White, J.D.L., Mcphie, J., Soule, S.A., 2015. In: Sigurdsson, H. (Ed.), Submarine lavas and hyaloclastite, en Encyclopedia of Volcanoes, second ed. Elsevier, Amsterdam, pp. 363–375.
Wilson, C.J.N., 2001. The 26.5 ka Oruanui eruption, New Zealand: an introduction and

overview. Journal of Volcanology and Geothermal Research 112 (1–4), 133–174.
Winchester, J.A., Floyd, P.A., 1977. Geochemical discrimination of different magma series and their differentiation product using immobile elements. Chemical Geology 20, 325–343.
Wohletz, K., Heiken, G., 1992. Volcanology and Geothermal Energy, First. ed. University of California Press, Berkeley.
Yoshihiko, G., Akihiko, T., 2019. Internal Structures and Growth Style of a Quaternary Subaerial Rhyodacite Cryptodome at Ogariyama, Usu Volcano, Hokkaido, Japan. Frontiers in Earth Science. https://doi.org/10.3389/feart.2019.00066.